Aqueous Liquid Crystals of Graphene Oxide

Zhen Xu and Chao Gao*

MOE Key Laboratory of Macromolecular Synthesis and Functionalization, Department of Polymer Science and Engineering, Zhejiang University, 38 Zheda Road, Hangzhou 310027, People's Republic of China

ABSTRACT The formation of liquid crystals (LCs) is the most viable approach to produce macroscopic, periodic self-assembled materials from oriented graphene sheets. Herein, we have discovered that well-soluble and single-layered graphene oxide (GO) sheets can exhibit nematic liquid crystallinity in water and first established their isotropic−nematic solid phase diagram *versus* mass fraction and salt concentration. The zeta potential of GO dispersion is around −64 mV, and its absolute value decreases with increasing salt concentration, implying that the electrostatic repulsive force between negatively charged GO sheets is the dominant interaction in the system of GO LCs and also explaining the salt-dependent phase behavior. For single-layer GO sheets with average diameter of 2.1 μm and polydispersity index of 83%, the isotropic−nematic phase transition occurs at a mass concentration of ∼0.025%, and a stable nematic phase forms at ∼0.5%. Rheological measurements showed that GO aqueous dispersions performed as typical shear flows and confirmed the isotropic−nematic transition. The ordering of GO sheets in aqueous dispersions and the solid state is demonstrated by the characterizations of polarized-light optical microscopy, small-angle X-ray scattering, scanning electron microscopy, and transmission electron microscopy. The direct, real-time fluorescent inspections by confocal laser microscopy further reveal that the individually dispersed fluorescent GO sheets align with orientational directions along their long axes. These novel findings shed light on the phase behaviors of diversely topological graphenes and lay the foundation for fabrication of long-range, ordered nano-objects and macroscopically assembled graphene-based functional materials.

KEYWORDS: graphene oxide · phase transition · nematic · liquid crystal · orientational ordering

Graphene is a single atomic plane of graphite, constructed with sp^2-hybridized carbon atoms in a perfect hexagonal lattice.[1] This thinnest known material is now receiving great attention, because of its unique attributes such as immense intrinsic mobility, the strongest mechanical strength ever measured, and record thermal conductivity, as well as promising applications, especially in electronics.[2−7] Besides the great progress made in research on the solid phase of graphene, recent exploration in graphene suspensions accessed by chemical functionalization has opened up a way to the liquid-phase chemistry of graphene.[8,9] For example, the aqueous suspensions of chemically oxidized graphene or graphene oxide (GO) can be processed into paper-like films that show high mechanical property.[10] However, achieving macroscopically ordered materials through self-organization or self-assembly of graphene sheets in a fluid phase is still a big challenge due to the lack of a scalable assembly method. It is known that fluid-phase assembly or the formation of lyotropic liquid crystals (LCs) is one of the most viable approaches to the production of large, oriented materials from nanoscale building blocks. It has been reported that carbon nanotubes (CNTs), another topology of anisotropic carbon nanostructures, could show nematic liquid crystalline behaviors in chlorosulfonic acid,[11] sulfuric acid,[12] and other solvents,[13] and their macroscopic, neat fibers fabricated from their mesophases exhibited good mechanical properties.[11,12,14] In addition, conical derivates of fullerene have also been found to be able to form polar LCs with interesting optical properties.[15]

Aside from the growing interest in the fabrication of oriented carboneous materials, the anisosymmetric inorganic colloidal particles (rods, plates, *etc.*) can also form various phases of lyotropic LCs,[16−18] which may in turn serve as a guide for orienting graphene sheets. For instance, CdSe and Au nanorods, the 1D counterparts of CNTs, could exhibit spontaneous isotropic (*I*)−nematic (*N*) phase transitions;[19,20] submicrometer-scale mineral platelets, the 2D counterparts of graphene sheets, can even show more complex mesophases in their suspensions including nematic, columnar, and lamellar phases, dependent on the volume fraction or concentration of colloidal particles.[21−28] Accordingly, we rationally speculate that graphene should be able to form LCs in a certain suspension. It is no doubt that the disclosure of liquid crystalline graphene and the determination of its mesophases will open up an avenue to

* Address correspondence to chaogao@zju.edu.cn.

Received for review December 17, 2010 and accepted March 4, 2011.

Published online March 04, 2011
10.1021/nn200069w

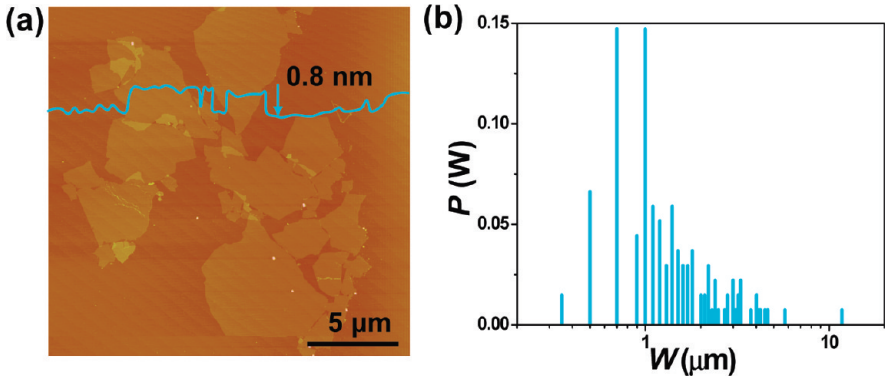

Figure 1. (a) Representative AFM height image of GO individual sheets deposited on mica from aqueous solution. (b) The width distribution $P(W)$ of GO sheets is counted and calculated from (a) and Figure S2. The number-average width $\langle W \rangle$ of the sheets is deduced as 2.1 μm, defining that the irregular sheets are regarded as squares of equal area, and the diameter of sheets is determined as the side length of the squares. The relative standard deviation (σ_w) is 83%, which is calculated according to $\sigma_w = (\langle W^2 \rangle - \langle W \rangle^2)/\langle W \rangle$. The average aspect ratio, or width/thickness ratio ($\langle W \rangle/\langle T \rangle$), of the GO sheets is calculated as 2.6×10^3.

liquid-phase physics of graphene and make the fabrication of long-range, ordered nano-objects and macroscopically periodic self-assembled structures of graphene accessible.

Two major aspects are considered to determine the possible formation of liquid crystalline graphene: aspect ratio (or width/thickness ratio) and sufficient dispersibility/solubility. Graphene sheets feature high anisotropy, with monatomic thickness (T) and normally micrometer-scale lateral width (W).[1] According to Onsager's theory,[29] such kind of ideal 2D sheet would capably form LCs in dispersions, when their volume fraction is higher than a critical value ($\Phi \approx 4T/W$). However, pristine graphene sheets are not soluble in water and poorly dispersible in common organic solvents (maximum mass fraction, f_m, $\sim 1 \times 10^{-5}$ in *N*-methylpyrrolidone (NMP) and $\sim 3 \times 10^{-5}$ in *ortho*-dichlorobenzene), owing to their strong $\pi-\pi$ stacking attraction.[30,31] Significantly, the solubility of graphene can be highly enhanced by chemical modification. In this regard, chemically oxidized graphene or graphene oxide (GO), possessing a similar anisotropic nature and comparable mechanical strength in bulk to pristine graphene,[10] has demonstrated good dispersibility in water and polar organic solvents such as *N*,*N*-dimethyl formamide (DMF) and NMP, due to the numerous oxygen-containing functional groups attached to its edges and two sides.[9] Despite its original insulation, GO can be easily converted into electrically conductive graphene by chemical and thermal reduction methods.[6,7,9] Moreover, GO gives the opportunity for further chemical functionalization, making it a major route to produce processable, multifunctional graphene and high-performance hybrids/composites.[6,7] Hence, LC of well-dispersible GO becomes more accessible especially in water and common organic solvents, in comparison with that of pristine graphene, which is scarcely wettable, and is of also extraordinary importance considering its surface functional groups suitable for chemical tailoring.

Here, we report that aqueous dispersions of single-layered GO can show isotropic−nematic ($I-N$) phase transition. The ordered orientational alignment in the nematic phase covers the fluid to solid state. For a deeper understanding, we have established a phase diagram of GO aqueous dispersion *versus* mass fraction and salt concentration. Our findings should facilitate large-scale alignment of graphene sheets in the fluid phase, open the way to long-range, ordered structures of graphene-based functional materials, and offer opportunities to uncover the complex phase behaviors of graphene with different topologies and its derivates immobilized with various chemical moieties.

RESULTS AND DISCUSSION

To access the possible LCs of GO, the most important step is to obtain highly soluble single-layered GO. We prepared GO by oxidization of natural graphite using $KMnO_4$ in concentrated H_2SO_4,[6,7] because this method is widely effective and has been used to obtain dispersible GO by many research groups.[8,9] Notably, compared to the classical Hummer's method,[32,33] we added an additional oxidization step to further enhance the solubility of GO sheets and improve the optical performance of GO dispersions. Compared with the conventional Hummer's GO, which generally features a deep brown color, low transmittance, weak fluorescence, and low zeta potential (−25 to −30 mV), our GO shows an orange color, higher transmittance, stronger fluorescence (about 4-fold larger than Hummer's GO), and higher zeta potential (−64 mV) (see Figure S1 for the details). The higher zeta potential of our GO indicates stronger repulsive forces between GO sheets, making the aqueous GO dispersions more stable; the higher transmittance and stronger fluorescence facilitate the optical observations on the dispersions.

As shown in Figure 1a and Figure S2, we used atomic force microscopy (AFM) characterization to confirm the

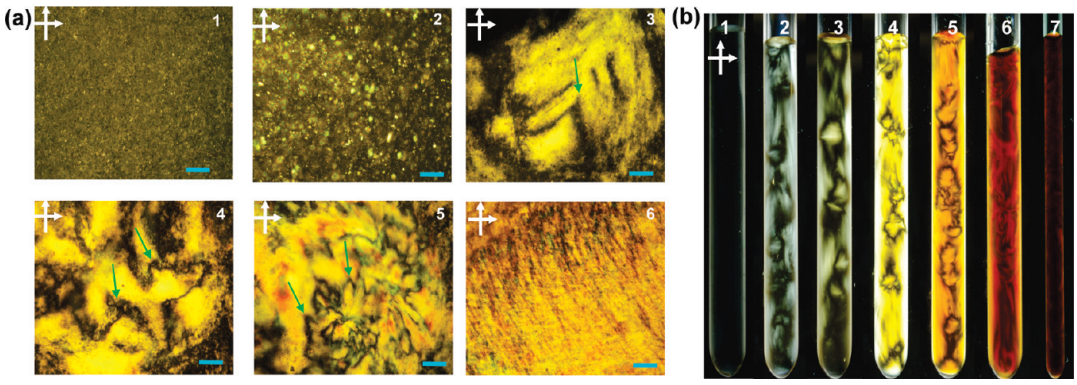

Figure 2. (a) POM microscopic images between crossed polarizers of GO aqueous dispersions in planar cells with f_m's of 5 × 10^{-4}, 1 × 10^{-3}, 3 × 10^{-3}, 5 × 10^{-3}, 8 × 10^{-3}, and 1.0 × 10^{-2} (from 1 to 6). The green arrows indicate the disclinations, and the scale bar represents 200 μm. (b) Macroscopic photographs between crossed polarizers of GO aqueous dispersions in test tubes with f_m's of 1.0 × 10^{-4}, 2.5 × 10^{-4}, 5 × 10^{-4}, 1.0 × 10^{-3}, 5 × 10^{-3}, 1.0 × 10^{-2}, and 2.0 × 10^{-2} (from 1 to 7).

complete exfoliations of graphite into individual sheets of single-layered GO. The individual anisotropic GO sheets have a uniform thickness (*T*) of 0.8 nm and an average lateral width (*W*) of 2.1 μm, with a corresponding average aspect ratio or width/thickness ratio (*W*/*T*) of 2.6 × 10^3. The polydispersity in width (σ_w) of GO sheets is counted statistically as 83%. The true thermodynamic aqueous solutions of GO are stable at their equilibrium state, due to the weaker $\pi-\pi$ stacking interactions and strong electrostatic repulsions between negatively charged sheets, confirmed by their negative zeta potential (−64 mV). Such an excellent solubility of single-layer GO should meet the prerequisite of high concentration to form a lyotropic LC and lay the foundation for our detailed studies on its possible liquid crystalline behavior.

It is well-recognized that the direct evidence of a lyotropic LC is the evolved birefringence between polarizers upon the dispersion concentration. Figure 2a shows the microscopic images of GO aqueous dispersions between crossed polarizers by polarized-light optical microscopy (POM). The emergence of isolated birefringence domains declares the *I*−*N* phase transition that starts at f_m as low as 2.5 × 10^{-4}, corresponding to a volume fraction of 1.9 × 10^{-4} (the experimental density of GO is 1.32 g·cm^{-3}).[34] Upon increasing f_m to 5 × 10^{-3}, the stable birefringence spreads the whole dispersions and displays vivid Schlieren texture, which is a typical texture of nematic phases. Singularities at the center of two-armed brushes are observed (marked by the arrows in Figure 2a), corresponding to the disclinations in the liquid crystalline structures.[13] The large area of Schlieren textures implies uniform orientational ordering in the samples. When the f_m increases to 1.0 × 10^{-2}, the textures change to parallel-banded structures, and we speculate that the liquid crystals evolve to more ordered mesophases such as lamellar phase, which is similar to lamellar LCs of montmorillonite platelets.[21]

Besides the POM observations, macroscopic colorful textures of colloidal LCs could be generally observed by the naked eye if the dispersions are placed between crossed polarizers. As shown in Figure 2b, no birefringence is observed for the dispersion with f_m of 1 × 10^{-4} (tube 1). When f_m is increased to 2.5 × 10^{-4}, the emergence of microscopic birefringence and thread-like textures indicates the preliminary formation of a nematic phase (tube 2). With increasing the concentration, the branches more closely resemble each other and the optical textures become more compact from tubes 3 to 7, and the birefringence becomes colorful starting from the dispersion in tube 5 with f_m of 5 × 10^{-3}, illustrating the formation of a uniform nematic phase. These macroscopic results intuitively affirm the *I*−*N* phase transition of aqueous GO dispersions. The phase separation was speeded up by centrifugation at 2000 rpm (340*g*) for 4 h followed by long-time (about one week) standing, and the equilibrium between diffusion and sedimentation resulted in two phases with a distinct interface (Figure S3-A). The upper phase is isotropic without birefringence, and the bottom phase shows spreading, colorful birefringence, a typical optical feature of LCs. Moreover, the volume percentage of the bottom nematic phase has a linear relationship with f_m ranging from 2.5 × 10^{-4} to 5 × 10^{-3} (Figure S3-B), exhibiting a similar phase-separation rule to that of colloidal mineral platelets.[23−26]

Considering the competition between orientational entropy and excluded volume entropy, the experimental and theoretical studies have elucidated that the polydispersity and aspect ratio are critical factors in the phase behaviors of anisotropic platelets and rods.[19−29,35,36] The isotropic−nematic phase coexistence of GO suspensions is observed in the f_m range of 2.5 × 10^{-4} to 5.0 × 10^{-3}, which is of the same order of magnitude as the simulated range (2.3 × 10^{-4} to 1.6 × 10^{-3}) for the polydisperse system of infinite platelets (*W*/*T* = 2.6 × 10^3 and σ_w = 83%).[35,36] In the frame of Onsager's theory, a higher anisotropy indicates a lower point of transitional concentration to an ordered mesophase, and this trend guides the preparation of

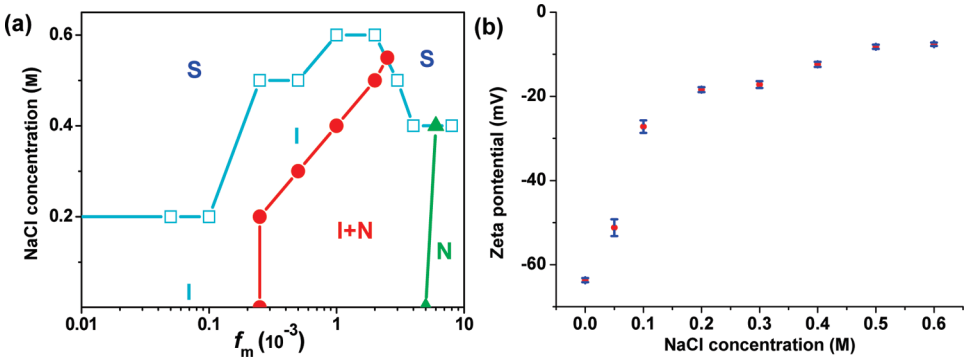

Figure 3. (a) Phase diagram of GO aqueous dispersions *versus* f_m and NaCl concentration. (b) Zeta potential of GO dispersions (f_m = 0.005) as a function of NaCl concentration.

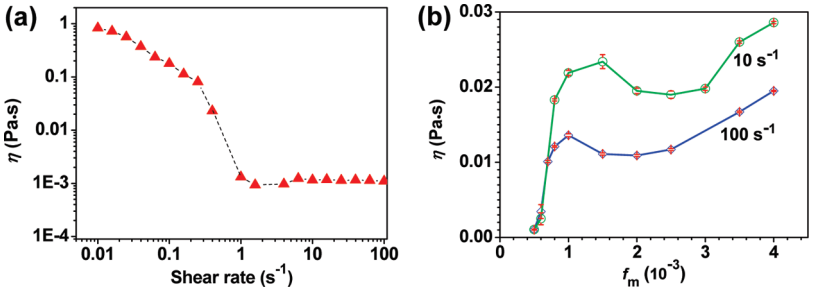

Figure 4. (a) Viscosity of GO aqueous dispersion with f_m of 5 × 10^{-3} as a function of shear rate. (b) Viscosity (η) under steady shearing as a function of f_m.

orderly structures in fluid phase at a relatively low amount; as to the polydispersity, a narrower size distribution should lead to a narrower range of transitional concentrations from *I* to *N* phase.[35] Indeed, we find that the starting f_m of the *I*−*N* transition of GO is located at the lowest range (~10^{-4}) because of its superior aspect ratio (~10^3), compared with the reported anisotropic mineral particles (Figure S4); the transitional concentration range is relatively broad because of the broad polydispersity of GO sheets.

To elucidate that the intrinsic electrostatic repulsive force plays a dominated role in the aqueous liquid crystalline system of GO sheets, we further established the phase diagram *versus* f_m and NaCl concentration (Figure 3a). In the absence of salt, GO dispersions evolve into three phases: isotropic (*I*, f_m < 2.5 × 10^{-4}), nematic (*N*, f_m > 5 × 10^{-3}), and biphasic coexistence (*I*+*N*). Traversing the phase diagram from bottom to top, flocculated solids (*S*) appear at salt concentrations of 0.2, 0.5−0.6, and 0.4 M, for the original *I*, *I*+*N*, and *N* phases, respectively. At low salt concentrations (<0.4 M), the biphasic domain is tilted toward higher f_m's. With increasing salt concentration, the biphasic phase turns into an *I* phase initially and *S* phase eventually, and the salt concentration of the transition to *I* phase scales with f_m of GO. In contrast, the single *N* phase flocculates directly. From the viewpoint of dominant interaction, the increasing concentration of salt weakens the repulsive forces and thus induces the phase evolution.[23] Such an explanation can be affirmed by tracking the zeta potentials of the dispersions along with the introduction of salt (Figure 3b). The absolute value of the zeta potential decreases from 64 to 7 mV with increasing salt concentration, and the ultimate flocculate inevitably occurs because of the minimized repulsive forces. All these results confirm the dominant electrostatic repulsion in GO aqueous dispersions.

Generally, the LC fluid structural information should be detectable by measurements of rheology[11,12] and small-angle X-ray scattering (SAXS).[23,24] From their rheological behaviors, GO aqueous dispersions signify typical shear flows and show decreased viscosity upon shearing (Figure 4a), likely because the anisotropic sheets are prone to align following flow surfaces. Each viscosity (η) curve displays a peak as a function of f_m, indicating the structures evolve from chaos to orientational ordering (Figure 4b).[11,12] The anisotropic 2D feature of GO sheets determines dilute transitional concentrations and extremely low η values even at very low shear rates (*e.g.*, 1 × 10^{-2} Pa·s at 10 s^{-1}), implying that alignment of GO is easily controllable by weak external forces. We believe that the low viscosity signifies an easy control for ordered graphene-based materials; for example strong GO materials could be made by the filtration flow.

Figure 5 shows the synchrotron SAXS results of different phases of GO dispersions. In the f_m range from 2.5 × 10^{-4} to 1 × 10^{-2}, the corresponding 2D patterns (Figure 5a, 1−3) evolve from a blank diffusive

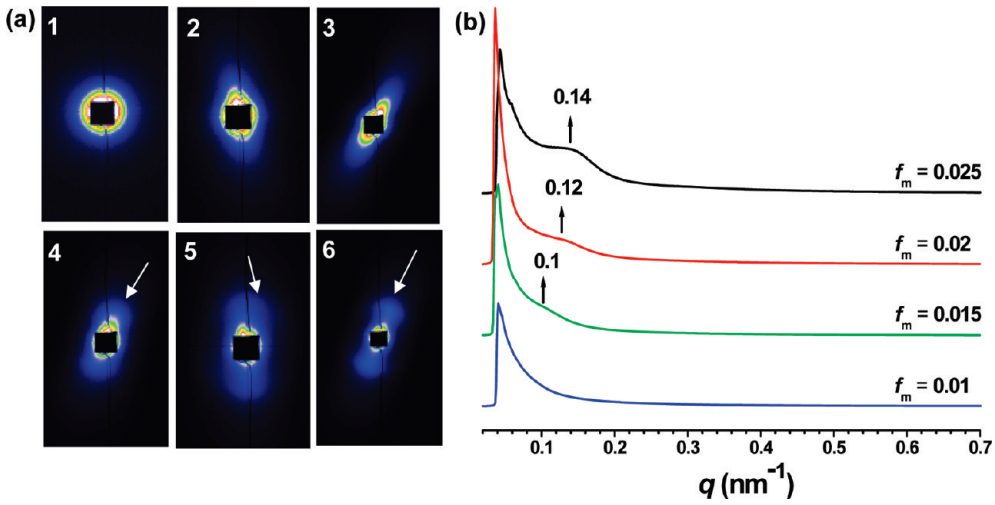

Figure 5. (a) SAXS 2D patterns of GO aqueous dispersions with f_m's of 2.5×10^{-4}, 5×10^{-3}, 1×10^{-2}, 1.5×10^{-2}, 2×10^{-2}, and 2.5×10^{-2}, from 1 to 6. The arrows in 4−6 indicate the diffuse arc and the scattering peak. (b) SAXS profiles of liquid crystals of GO with high concentrations ($f_m \geq 1 \times 10^{-2}$). The spectra depict the scattering intensity as a function of scattering vector q ($q = (4\pi \sin \theta)/\lambda$, where 2θ is the scattering angle).

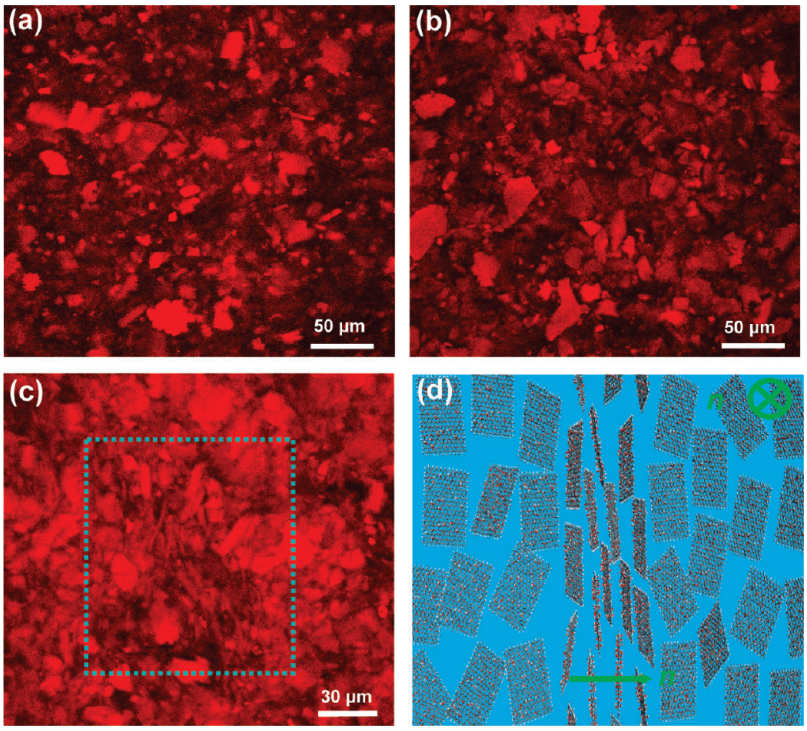

Figure 6. Real-time confocal laser microscopy inspections of GO aqueous dispersions. Their f_m's are 2.5×10^{-4} (a), 5.0×10^{-3} (b), and 1×10^{-2} (c). A model (d) depicts the rotation of orientation vectors (n) in (c); the arrow directs the vector (n) on the paper, and the cross indicates the one into the paper.

signal ($f_m = 2.5 \times 10^{-4}$) to an elliptical diffusive pattern ($f_m = 5 \times 10^{-3}$) and an elliptical pattern with a larger axial ratio ($f_m = 1 \times 10^{-2}$), indicating the increasing degree of orientation in the GO LCs with enlarging the content of the GO. Simultaneously, no diffuse arc is observed in the patterns at low f_m ($<1 \times 10^{-2}$), indicating the sole orientational ordering in the nematic phase. By contrast, in the higher f_m range ($f_m > 1 \times 10^{-2}$), the corresponding 2D patterns (Figure 5a, 4−6) exhibit typical diffusive arcs, which are ascribed to the Bragg reflection. We propose that the nematic phase of GO should evolve to a lamellar phase that has positional ordering at a higher concentration of GO sheets. The profiles in Figure 5b give detailed information on positional ordering as a function of concentration. The diffusive peak at $q = 0.1-0.14$ nm^{-1} for $f_m \geq 1.5 \times 10^{-2}$ could be assigned to a (100) reflection with a corresponding spacing ($d = 2\pi/q$) between GO sheets

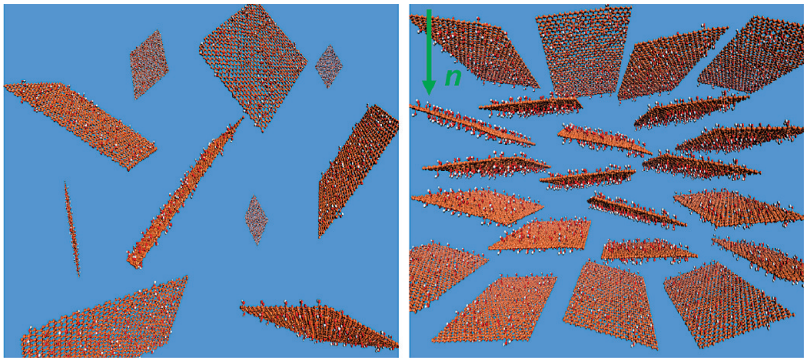

Figure 7. Schematic models for isotropic (left) and nematic (right) phases of GO aqueous dispersions. GO sheets randomly distribute in isotropic phase and align with an orientation vector (*n*) perpendicular to the sheet planes in the nematic phase.

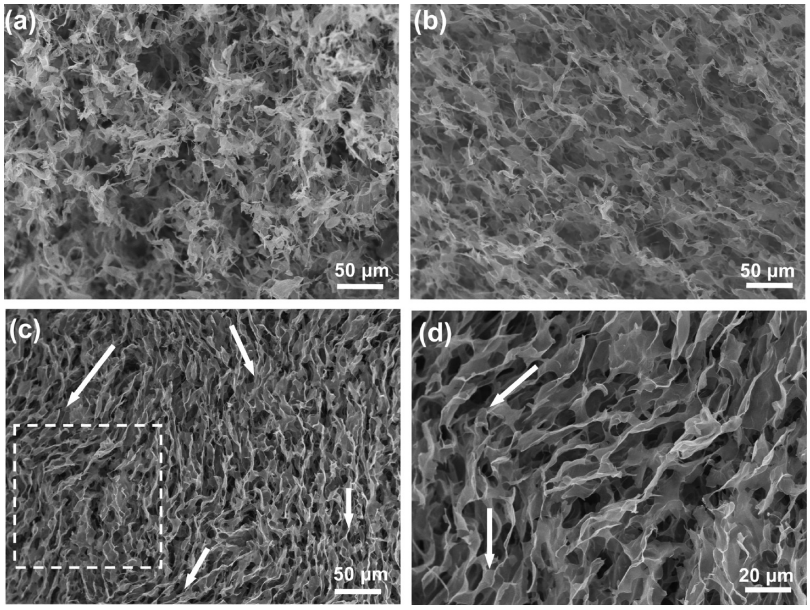

Figure 8. SEM images of GO freeze-dried foams. The original f_m's are (a) 1×10^{-4}, (b) 2.5×10^{-3}, and (c, d) 1.0×10^{-2}. The marked area in (c) is zoomed in as (d); and the arrows in (c) and (d) indicate the alignment directions of the GO sheets.

in the lamellar phase. According to the 1D swollen model of the lamellar phase,[24] the interlayer spacing can be calculated by $d = T/\Phi$ (Φ is the volume fraction). In this context, we estimated the d values ($T = 0.8$ nm) are around 41.6, 52.0, and 69.3 nm at their respective f_m of 2.5×10^{-2}, 2×10^{-2}, and 1.5×10^{-2}. These d values are approximately coincident with our experimental results, in which the d values obtained from the SAXS diffusive peak are 45, 52, and 63 nm at f_m's of 2.5×10^{-2}, 2×10^{-2}, and 1.5×10^{-2}, respectively. We conclude that the $d_{(100)}$ value decreases with increasing f_m of GO, which is a general rule in the lamellar phases of 2D colloidal particles.[23,24] In a word, the SAXS results definitely demonstrate the orientation and lamellar orderings in the respective nematic and lamellar phases of GO, depending on the concentration.

Furthermore, our GO sheets are highly fluorescent under visible light (see Figure S1c for the fluorescent spectra), which makes possible the direct inspection of the inner textures of GO dispersions in their original states. Figure 6a–c shows the real-time observations revealing the orientational ordering in the nematic phase of GO by confocal laser microscopy. The aligned GO sheets favor orientational vectors (n) perpendicular to their sheets planes. Increasing f_m to 5×10^{-3}, the dispersions exhibit more orderly textures, because of the expanding nematic phase (Figure 6a,b). In the neat nematic phase, the red-fluorescent sheets align into two main patterns with their orientation vectors being vertical and parallel to the focal plane, respectively (Figure 6c). This rotation of such n's is induced by topological defects, as depicted by the model shown in Figure 6d.

On the basis of the I–N phase transition of GO aqueous dispersions proven above, we provide respective models for their I and N phases (Figure 7). GO sheets show a chaotic distribution in dilute dispersions (I phase) whereas ordered alignments in the concentrated N phase favoring orientation vectors.

Since the LCs of GO dispersions have been validated, we investigated the textures of organized

solids, by scanning electron microscopy (SEM) and transmission electron microscopy (TEM). The freeze-dried solid derived from the isotropic dispersion shows disordered clusters consisting of curly GO sheets (Figure 8a), and the one from the biphasic phase displays orientational domains surrounded by irregular clusters (Figure 8b). In the neat *N*-phasic solid, ordered alignments of GO sheets along their planar axes are clearly observed, with deflected orientational directions as marked by arrows (Figure 8c,d). Similarly, we also identified the disorderly dispersed and ordered organized textures of *I* and *N* phases by TEM (Figure S5).

CONCLUSIONS

Recently, Behabtu *et al.* reported the dispersions of graphite in superacid of chlorosulfonic acid, providing a protocol to obtain graphene sheets. They also showed a preliminary POM observation for the Schlieren textures of liquid crystalline graphene in the superacid at a high concentration ($f_m = 2$).[37] Herein, we have confirmed the liquid crystalline behaviors of chemically modified graphene in water by various important characterization methods and found that the nematic phase of GO sheets could evolve to lamellar phase upon increasing GO concentration.

The combination of LC and the highly reactive character of GO encourages us to explore liquid crystals of chemically functionalized graphene sheets for the engineering of diverse macroscopic ordering materials with tailored properties, such as neat graphene and composite fibers, which could lead to different technological applications. The LC can find new optical functions of graphene and graphene-based macroscopic ordered materials. The aqueous surrounding of GO LCs also provides the foundation for its biological applications, especially for the fabrication of highly ordered, self-assembled chiral biomolecules/graphene conjugates. Single atom thick graphene provides an ideal model for the liquid crystal theory and simulations, allowing the advancement of fluid-phase theory of graphene. We believe that our findings can also enlighten the exploitation of the fascinating liquid crystal family of graphene with different topologies (ribbons, scrolls, *etc.*), size, layers, polydispersity, and immobilized chemical moieties.

EXPERIMENTAL METHODS

Materials. Graphite powder (40 μm) was obtained from Qingdao Henglide Graphite Co., Ltd. Concentrated H_2SO_4 (98%) and $KMnO_4$ were purchased from Sinopharm Chemical Reagent Co., Ltd. and used as received.

Synthesis of GO. In the preoxidation step, concentrated H_2SO_4 (40 mL) was added into a 500 mL round-bottom flask and heated to 80 °C. $K_2S_2O_8$ (8.4 g) and P_2O_5 (8.4 g) were added successively, followed by slow addition of graphite powder (10 g). The mixture was kept at 80 °C for 4.5 h. After cooling to room temperature, the mixture was diluted with deionized water and left overnight. Then the mixture was vacuum-filtered and washed with deionized water (1.6 L) using a 0.22 μm polycarbonate membrane. The solid was dried in air at room temperature. In the second oxidation step, a 1.5 L three-necked round-bottom flask containing 230 mL of concentrated H_2SO_4 was chilled to 0 °C. The preoxidized sample was added into the flask and stirred. Then, $KMnO_4$ (60 g) was added slowly under continuous stirring, and the temperature was kept below 10 °C. The mixture was heated to 35 °C and stirred for 2 h. The mixture was then diluted with deionized water (0.5 L) and stirred for 2 h. Successively, an additional 1.5 L of deionized water was added, followed by dropwise addition of 30% H_2O_2 (25 mL). The mixture was left undisturbed for 4 days, and the nearly clear supernatant was decanted. The precipitate mixture was repeatedly washed with water and centrifuged successively with 1 M HCl solution at least three centrifugation cycles to remove residual metal oxides and then washed with deionized water until the decantate became neutral, followed by ultrasonication for 30 min. The deep brown solids were obtained by centrifugation and drying under vacuum. To further enhance the solubility of oxidized graphene sheets and improve the optical performance of GO dispersions, the as-prepared oxidized graphene sheets (5 g) were redispersed in concentrated H_2SO_4 (100 mL), and $KMnO_4$ (25 g) was introduced at room temperature, followed by stirring for 20 min. After the introduction of H_2O_2 (5 mL) and repeated washing with 1 M HCl solution and deionized water to neutral again, we obtained a pale orange aqueous dispersion of resultant GO (Figure S1).

Preparation of GO Solid Samples from Aqueous Solutions by Freeze-Drying. The aqueous dispersions of GO were loaded in beakers (for SEM) or dropped onto copper grids (for TEM) and quenched in liquid nitrogen. The freezing solids were quickly transferred to the vacuum freeze-dryer and kept at −60 °C until completely dried. The fluffy solids were carefully put on flat substrates precoated with carbonic glues for SEM characterizations.

Characterization. AFM images of GO sheets were taken in the tapping mode on a Nano Scope IIIA, with samples prepared by spin-coating from diluted aqueous solutions onto freshly exfoliated mica substrates at 1000 rpm. SEM images were taken on a Hitachi S4800 field-emission SEM system. TEM was performed on a JEM-1200EX with an accelerating voltage of 120 kV. SAXS tests were carried out at Shanghai Synchrotron Radiation Facility (SSRF), by using a fixed wavelength of 0.124 nm, a sample to detector distance of 5 m, and an exposure time of 300 s. The scattering patterns were collected on a CCD camera, and the curve intensities *vs q* were obtained by integrating the data from the patterns. Rheological measurements were carried out on a TA AR-C12 instrument. The measurements were taken at 25 ± 0.2 °C. The relationships of viscosity *vs* shear rate were obtained from the mode of steady flow, and the relationships of the viscosity *vs* mass fraction of aqueous dispersion were obtained from the mode of peak holding at different shear rates. POM observations were performed with a Nikon E600POL, and the liquid samples were loaded into the planar cells. Confocal observations were performed on a Zeiss Lsm510 microscope, using a 488 nm laser for excitation with a filtrate around 560 nm. The measurement of zeta potential was performed on a ZET-3000HS apparatus.

Acknowledgment. We thank Prof. Sir Harry Kroto, Dr. M. Hanif, and Dr. Y. Z. Jin for helpful discussions. We also thank SSRF for the help with SAXS characterizations. This work was supported by the National Natural Science Foundation of China (No.

20974093), the National Key Basic Research Program of China (973 Program) (No. 2007CB936000), Qianjiang Talent Foundation of Zhejiang Province (No. 2010R10021), the Fundamental Research Funds for the Central Universities (No. 2009QNA4040), Zhejiang Provincial Natural Science Foundation of China (No. R4110175), and Research Fund for the Doctoral Program of Higher Education of China (No. 20100101110049).

Supporting Information Available: Detailed characterization of GO, macroscopic photos of phase separation, statically listed data from the literature, and TEM images are available free of charge *via* the Internet at http://pubs.acs.org.

REFERENCES AND NOTES

1. Novoselov, K. S.; Geim, A. K.; Morozov, S. V.; Jiang, D.; Zhang, Y.; Dubonos, S. V.; Grigorieva, I. V.; Filrsov, A. A. Electric Field Effect in Atomically Thin Carbon Films. *Science* **2004,** *306*, 666–669.
2. Geim, K. Graphene: Status and Prospects. *Science* **2009,** *324*, 1530–1534.
3. Allen, M. J.; Tung, V. C.; Kaner, R. B. Honeycomb Carbon: A Review of Graphene. *Chem. Rev.* **2010,** *110*, 132–145.
4. Rao, C. N. R.; Sood, A. K.; Subrahmanyam, K. S.; Govindaraj, A. Graphene: The New Two-Dimensional Nanomaterial. *Angew. Chem., Int. Ed.* **2009,** *48*, 7752–7777.
5. Stankovich, S.; Dikin, D.; Dommett, G. H. B.; Kohlhaas, K. M.; Zimney, E. J.; Stach, E. A.; Piner, R. D.; Nguyen, S. T.; Ruoff, R. S. Graphene-based Composite Materials. *Nature* **2006,** *442*, 282–286.
6. He, H. K.; Gao, C. General Approach to Individually Dispersed, Highly Soluble, and Conductive Graphene Nanosheets Functionalized by Nitrene Chemistry. *Chem. Mater.* **2010,** *22*, 5054–5064.
7. Xu, Z.; Gao, C. *In Situ* Polymerization Approach to Graphene-Reinforced Nylon-6 Composites. *Macromolecules* **2010,** *43*, 6716–6723.
8. Park, S.; Ruoff, R. S. Chemical Methods for the Production of Graphenes. *Nat. Nanotechnol.* **2009,** *4*, 217–224.
9. Dreyer, D. R.; Park, S.; Bielawski, C. W.; Ruoff, R. S. The Chemistry of Graphene Oxide. *Chem. Soc. Rev.* **2010,** *39*, 228–240.
10. Dikin, D. A.; Stankovich, S.; Zimney, E. J.; Piner, R. D.; Dommett, G. H. B.; Evmenenko, G.; Nguyen, S. T.; Ruoff, R. S. Preparation and Characterization of Graphene Oxide Paper. *Nature* **2007,** *448*, 457–460.
11. Davis, V. A.; Parra-Vasquez, A. N. G.; Green, M. J.; Rai, P. K.; Behabtu, N.; Prieto, V.; Booker, R. D.; Schmidt, J.; Kesselman, E.; Zhou, W.; *et al.*True Solutions of Single-Walled Carbon Nanotubes for Assembly into Macroscopic Materials. *Nat. Nanotechnol.* **2009,** *4*, 830–834.
12. Ericson, L. M.; Fan, H.; Peng, H. Q.; Davis, V. A.; Zhou, W.; Sulpizio, J.; Wang, Y. H.; Booker, R.; Vavro, J.; Guthy, C.; *et al.* Macroscopic, Neat, Single-Walled Carbon Nanotube Fibers. *Science* **2004,** *305*, 1447–1450.
13. Song, W. H.; Kinloch, I. A.; Windle, A. H. Nematic Liquid Crystallinity of Multiwall Carbon Nanotubes. *Science* **2003,** *302*, 1363.
14. Zhang, S. J.; Kumar, S. Carbon Nanotubes as Liquid Crystals. *Small* **2008,** *4*, 1270–1283.
15. Sawamura, M.; Kawai, K.; Matsuo, Y.; Kanie, K.; Kato, T.; Nakamura, E. Stacking of Conical Molecules with a Fullerene Apex into Polar Columns in Crystals and Liquid Crystals. *Nature* **2002,** *419*, 702–705.
16. Davidson, P.; Gabriel, J. C. P. Mineral Liquid Crystals. *Curr. Opin. Colloid Interface Sci.* **2005,** *9*, 337–383.
17. Sonin., A. S. Inorganic Lyotropic Liquid Crystals. *J. Mater. Chem.* **1998,** *8*, 2557–2574.
18. Davidson, P.; Batail, P.; Gabriel, J. C. P.; Livage, J.; Sanchez, C.; Bourgaux., C. Mineral Liquid Crystalline Polymers. *Prog. Polym. Sci.* **1997,** *22*, 913–936.
19. Li, L. S.; Walda, J.; Manna, L.; Alivisatos, A. P. Semiconductor Nanorod Liquid Crystals. *Nano Lett.* **2002,** *2*, 557–560.
20. Murphy, C. J.; Jana, N. R. Liquid Crystalline Assemblies of Ordered Gold Nanorods. *J. Mater. Chem.* **2002,** *12*, 2909–2912.
21. Emerson., W. H. Liquid Crystals of Montmorillonite. *Nature* **1956,** *178*, 1248–1249.
22. Gabriel, J. C. P.; Sanchez, C.; Davidson, P. Observation of Nematic Liquid-Crystal Textures in Aqueous Gels of Smectite Clays. *J. Phys. Chem.* **1996,** *100*, 11139–11143.
23. Michot, L. J.; Bihannic, I.; Maddi, S.; Funari, S. S.; Baravian, C.; Levitz, P.; Davidson, P. Liquid-Crystalline Aqueous Clay Suspensions. *Proc. Natl. Acad. Sci.* **2006,** *103*, 16101–16104.
24. Gabriel, J. C. P.; Camerel, F.; Lemaire, B. J.; Desvaux, H.; Davidson, P.; Batail, P. Swollen Liquid-Crystalline Lamellar Phase Based on Extended Solid-like Sheets. *Nature* **2001,** *413*, 504–508.
25. Miyamoto, N.; Nakato, T. Liquid Crystallinity of Layered Niobate $K_4Nb_6O_{17}$. *Adv. Mater.* **2002,** *14*, 1267–1270.
26. Liu, S. Y.; Zhang, J.; Wang, N.; Liu, W. R.; Zhang, C. G.; Sun, D. J. Liquid-Crystalline Phases of Colloidal Dispersions of Layered Double Hydroxides. *Chem. Mater.* **2003,** *15*, 3240–3241.
27. Mourad, M. C. D.; Devid, E. J.; van Schooneveld, M. M.; Vonk, C.; Lekkerkerker, H. N. W. Formation of Nematic Liquid Crystals of Sterically Stablized Layered Double Hydroxide Platelets. *J. Phys. Chem. B* **2008,** *112*, 10141–10152.
28. van der Kooij, F. M.; Kassapidou, K.; Lekkerkerker, H. N. W. Liquid Crystal Phase Transitions in Suspensions of Polydisperse Plate-like Particles. *Nature* **2000,** *406*, 868–871.
29. Onsager, L. The Effect of Shape on the Interaction of Colloidal Particles. *Ann. N.Y. Acad. Sci.* **1949,** *51*, 627–659.
30. Hernandez, Y.; Nicolos, V.; Lotya, M.; Blighe, F. M.; Sun, Z.; De, S.; Mcgovern, I. T.; Holland, B.; Byrne, M.; Gun'Ko, Y. K.; *et al.* High-Yield Production of Graphene by Liquid-Phase Exfoliation of Graphite. *Nat. Nanotechnol.* **2008,** *3*, 563–568.
31. Hamilton, C. E.; Lomeda, J. R.; Sun, Z. Z.; Tour, J. M.; Barron, A. R. High-Yield Organic Dispersions of Unfunctionalized Graphene. *Nano Lett.* **2009,** *9*, 3460–3462.
32. Hummers, W. S.; Offeman, R. E. Preparation of Graphitic Oxide. *J. Am. Chem. Soc.* **1958,** *80*, 1339.
33. Kovtyukhova, N. I.; Ollivier, P. J.; Martin, B. R.; Mallouk, T. E.; Chizhik, S. A.; Buzaneva, E. V.; Gorchinskiy, A. D. Layer-by-Layer Assembly of Ultrathin Composite Films from Micron-Sized Graphite Oxide Sheets and Polycations. *Chem. Mater.* **1999,** *11*, 771–778.
34. Sun, X. M.; Luo, D. C.; Liu, J. F.; Evans, D. G. Monodisperse Chemically Modified Graphene Obtained by Density Gradient Ultracentrifugal Rate Separation. *ACS Nano* **2010,** *4*, 3381–3389.
35. Bates, M. A.; Frenkel, D. Nematic-Isotropic Transition in Polydisperse Systems of Infinitely Thin Hard Platelets. *J. Chem. Phys.* **1999,** *10*, 6553–6559.
36. Veerman, J. A. C.; Frenkel, D. Phase Behavior of Disklike Hard-Core Mesogens. *Phys. Rev. A* **1992,** *45*, 5632–5648.
37. Behabtu, N.; Lomeda, J. R.; Green, M. J.; Higginbotham, A. L.; Sinitskii, A.; Kosynkin, D. V.; Tsentalovich, D.; Parra-Vasquez, A. N. G.; Schmidt, J.; Kesselman, E.; *et al.* Spontaneous High-Concentration Dispersions and Liquid Crystals of Graphene. *Nat. Nanotechnol.* **2010,** *5*, 406–411.